Global Biogeochemical Cycles

RESEARCH ARTICLE
10.1029/2021GB006969

Dimethyl Sulfide-Induced Increase in Cloud Condensation Nuclei in the Arctic Atmosphere

Ki-Tae Park[1,2], Young Jun Yoon[1], Kitack Lee[3], Peter Tunved[4], Radovan Krejci[4], Johan Ström[4], Eunho Jang[1,2], Hyo Jin Kang[1,2], Sehyun Jang[3], Jiyeon Park[1], Bang Yong Lee[1], Rita Traversi[5,6], Silvia Becagli[5,6], and Ove Hermansen[7]

[1]Korea Polar Research Institute, Incheon, South Korea, [2]University of Science and Technology, Daejeon, South Korea, [3]Department of Environmental Science and Engineering, Pohang University of Science and Technology, Pohang, South Korea, [4]Department of Environmental Science and Analytical Chemistry & Bolin Centre for Climate Research, Stockholm University, Stockholm, Sweden, [5]Department of Chemistry "Ugo Schiff", University of Florence, Sesto Fiorentino, Italy, [6]Institute of Polar Science, ISP-CNR, Venezia Mestre, Italy, [7]Norwegian Institute for Air Research, Kjeller, Norway

Key Points:

- Dimethyl sulfide (DMS), aerosol particle numbers, and cloud condensation nuclei (CCN) were measured in the Arctic atmosphere
- Multiple episodes of new particle formation and particle growth with both high and low DMS mixing ratios were observed
- An increase in CCN was observed when the formation and growth of aerosol particles derived from DMS occurred

Supporting Information:

Supporting Information may be found in the online version of this article.

Correspondence to:

K.-T. Park,
ktpark@kopri.re.kr

Citation:

Park, K.-T., Yoon, Y. J., Lee, K., Tunved, P., Krejci, R., Ström, J., et al. (2021). Dimethyl sulfide-induced increase in cloud condensation nuclei in the Arctic atmosphere. *Global Biogeochemical Cycles*, *35*, e2021GB006969. https://doi.org/10.1029/2021GB006969

Received 3 FEB 2021
Accepted 14 JUN 2021

Abstract Oceanic dimethyl sulfide (DMS) emissions have been recognized as a biological regulator of climate by contributing to cloud formation. Despite decades of research, the climatic role of DMS remains ambiguous largely because of limited observational evidence for DMS-induced cloud condensation nuclei (CCN) enhancement. Here, we report concurrent measurement of DMS, physiochemical properties of aerosol particles, and CCN in the Arctic atmosphere during the phytoplankton bloom period of 2010. We encountered multiple episodes of new particle formation (NPF) and particle growth when DMS mixing ratios were both low and high. The growth of particles to sizes at which they can act as CCN accelerated in response to an increase in atmospheric DMS. Explicitly, the sequential increase in all relevant parameters (including the source rate of condensable vapor, the growth rate of particles, Aitken mode particles, hygroscopicity, and CCN) was pronounced at the DMS-derived NPF and particle growth events. This field study unequivocally demonstrates the previously unconfirmed roles of DMS in the growth of particles into climate-relevant size and eventual CCN activation.

Plain Language Summary Marine phytoplankton can produce gaseous dimethyl sulfide (DMS), which is the most abundant form of sulfur released into the atmosphere through sea-air gas exchange. The polar oceans are known to be the most productive ocean in terms of DMS due to the high abundance of DMS-producing phytoplankton. The oceanic emission of DMS into the marine atmosphere has received substantial attention during the last 30 years because of its contribution to cloud formation and its subsequent impact on climate. However, the climate feedback role of DMS remains uncertain due to insufficient evidence supporting DMS-derived formation of aerosol particles and their subsequent activation into cloud condensation nuclei (CCN), in turn affecting the Earth's radiation budget. In this study, we analyzed atmospheric DMS mixing ratios, and concentrations of aerosol particles and CCN in the Arctic atmosphere during the phytoplankton bloom period. Our results show that atmospheric DMS affects the formation and growth of aerosol particles and significantly contributes to CCN populations.

1. Introduction

Aerosols are an integral part of the global climate system, scattering and absorbing incoming radiation and forming cloud condensation nuclei (CCN; Carslaw et al., 2013). Marine aerosols contribute significantly to the global aerosol load and consequently impact the Earth's radiative budget (O'Dowd & De Leeuw, 2007). The atmospheric oxidation of dimethyl sulfide (DMS) derived from marine phytoplankton is the most abundant source of naturally occurring sulfate aerosol particles (Simó, 2001). Owing to their high hygroscopicity, sulfur-containing compounds are important for the formation of aerosol particles and contribute to the population of CCN (Boy et al., 2005; Kulmala, 2003). More than 30 years ago, Charlson et al. (1987) proposed a biological regulation of the climate system that could be initiated by a warming-induced increase in oceanic DMS emissions (the so-called CLAW hypothesis). This hypothesis postulated that DMS-derived sulfate aerosols made up the majority of the CCN in the marine atmosphere; therefore, an increase in DMS emissions

would result in an increase in CCN and a decrease in the amount of solar radiation reaching Earth's surface. Thus, reducing the source of DMS again.

New particle formation (NPF), which is characterized by a burst of high concentration of nanometer-size particles, is the dominant source of the total aerosol particle number concentration and evolves to CCN in the global troposphere (Kerminen et al., 2018; Kim et al., 2019; S.-H. Lee et al., 2019). Recent studies performed in remote polar regions revealed that biogenic DMS emissions significantly contribute to the formation of new particles during the biologically productive periods (Chang et al., 2011; Jang et al., 2019; K.-T. Park et al., 2017). However, the relationship between DMS-derived NPF and subsequent growth to CCN has not been clearly constrained (Ayers & Cainey, 2007; Brooks & Thornton, 2018; Quinn & Bates, 2011; Yoon & Brimblecombe, 2002), mainly due to the absence of simultaneous measurements of these compounds in remote marine environments. Moreover, these processes are affected by a variety of meteorological parameters and properties of pre-existing particles (Kerminen et al., 2018; Kulmala & Kerminen, 2008; S.-H. Lee et al., 2019); thus, it is difficult to single out the effect of biogenic precursors, including DMS, on Earth's climate under ongoing marine environmental changes (Carslaw et al., 2013; Quinn & Bates, 2011; Wang et al., 2018; Woodhouse et al., 2010, 2013).

Marine DMS emissions show distinct seasonal and latitudinal variability as the production of DMS and its precursor compound (dimethylsulfoniopropionate; DMSP) in the ocean is highly species-specific (Lana et al., 2011; K.-T. Park et al., 2014). The Arctic and Antarctic oceans are known to be the hotspots of DMS emissions because DMS-producing phytoplankton are abundant in these regions (Kettle et al., 1999; Levasseur, 2013). The Arctic Ocean is currently warming and acidifying faster than other marine environments (K. Lee et al., 2011; Stroeve et al., 2007), and the resulting environmental changes (e.g., decreases in sea-ice extent, mixed-layer shallowing, increases in sea surface temperature, eutrophication, and decreases in pH) may affect the emission of biogenic DMS by changing the biomass and taxonomic composition of marine phytoplankton in these fragile regions (Hopkins et al., 2020; Levasseur, 2013). Long-term field measurements of methanesulfonic acid (MSA, oxidative product of DMS) in three Arctic sites (Alert, 82.5°N, 62.3°W; Barrow, 71.2°N, 156.4°W; Zeppelin, 78.5°N, 11.8°E) showed that MSA concentration in aerosol particles increased at a rate of 40%–80% decade^{-1} between 1998 and 2009 due to the northward migration of the biologically active marginal ice zone (Sharma et al., 2012). A recent satellite-based study also reported that DMS emissions in the Arctic Ocean have increased at a rate of 10 Gg S decade^{-1} (>30% decade^{-1}), mainly as a result of increases in the extent of open water (Galí et al., 2019). The increasing marine emission of DMS and resulting changes in microphysical properties of marine aerosols and clouds could possibly moderate Arctic warming. To address this issue, observational evidence to support the DMS-induced enhancement of CCN formation is crucial.

In this study, we report atmospheric DMS mixing ratios, MSA concentrations, number concentrations and size distributions of aerosol particles, and CCN concentrations at Ny-Ålesund, Svalbard (78.5°N, 11.8°E) during the phytoplankton bloom period (April–June) in 2010. The relationship between these components were investigated by comparing NPF and particle growth events that occurred during episodes of observed high and low DMS mixing ratios. The results are used to address the link between DMS, aerosols, and CCN-production during the Arctic spring period.

2. Materials and Methods

2.1. DMS and MSA Measurements

The atmospheric DMS mixing ratios were measured at hourly intervals from April 11 to June 10, 2010 at the Zeppelin observatory, which is located 2 km southwest of the small settlement of Ny-Ålesund at an elevation of 474 m above sea level (m.a.s.l.; Figure 1a). The analytical system used includes a component for DMS trapping and elution and a gas chromatograph (GC) equipped with a pulsed flame photometric detector enabling the quantification of trace level DMS. Details of the DMS analytical system and the DMS measurement protocol are described in S. Jang et al. (2016).

For the measurement of MSA, an air sampler equipped with a PM_{10} impactor (collecting particles <10 μm in aerodynamic equivalent diameter) was used to collect aerosol particles. The inlet of the sampler was mounted on the roof of the Gruvebadet observatory (1 km southwest of the Ny-Ålesund settlement and

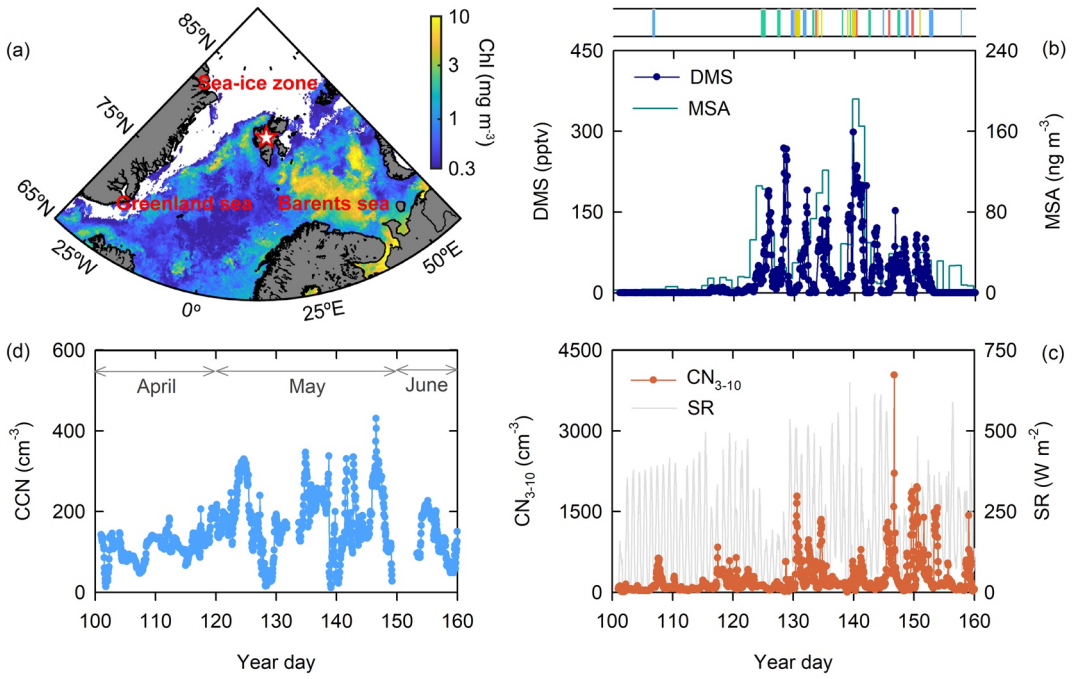

Figure 1. (a) Mean chlorophyll concentration during the study period (April–June 2010). Star symbol indicates the location of the Svalbard observation site (78.5°N, 11.8°E). (b) Atmospheric dimethyl sulfide (DMS) mixing ratios (blue circles) and methanesulfonic acid concentrations (green line). (c) Hourly median values of the number concentrations of nanoparticles ($CN_{3–10}$; 3–10 nm in diameter; red circles) and solar irradiance (gray line). (d) Hourly median values of the number concentrations of cloud condensation nuclei (CCN at 0.4% supersaturation). The color bars above Figure 1b indicate where cases have been assigned to time periods (blue for case A, high new particle formation (NPF) and low DMS; red for case B, high NPF and high DMS; yellow for case C, moderate NPF and high DMS; green for case D, low NPF and high DMS).

60 m.a.s.l.) and samples were taken every 24 h during the study period. Aerosol particles were collected on Teflon filters (PALL Gelman) at a flow rate of 2.3 m^3 h^{-1}. The MSA collected on the filter was extracted into 10 mL of Milli-Q water, and their concentrations determined using ion chromatography (Dionex, Thermo Fisher Scientific Inc.) as described by Becagli et al. (2016).

2.2. Aerosol Measurements

The physical properties of the aerosol particles (number concentration, size distribution, and CCN concentration) were also concurrently measured at the Zeppelin observatory. The number concentration of aerosol particles (CN) was measured using two condensation particle counters (CPCs) at 1 min intervals with different cut-off diameters: particles larger than 3 nm (CN_3; TSI model 3025), particles larger than 10 nm (CN_{10}; TSI model 3010). The number concentration of nanoparticles (between 3 and 10 nm in diameter; $CN_{3–10}$), which indicate the existence of newly formed particles via gas-to-particle conversion, was estimated using the difference in the number concentrations of aerosol particles between the two CPCs. The size distribution of aerosol particles ranging from 10 to 560 nm in mobility equivalent diameter were analyzed using a differential mobility particle analyzer (DMPS), consisting of a medium size Hauke differential mobility analyzer in combination with a CPC (TSI model 3010), with a time resolution of 10 min. The Droplet Measurement Technologies CCN counter was used to measure the CCN concentration at various supersaturations (0.2%, 0.4%, 0.6%, 0.8%, and 1.0%). Each supersaturation level (except for 0.2%) was measured for 5 min. CCN concentration at supersaturation of 0.2% was measured for 10 min. Hourly median values for number concentration of particles measured by CPCs, DMPS, and CCN counter were used for the further analysis. A more detailed description regarding the measurement of aerosol particles is given in Jung et al. (2018).

2.3. Estimation of Parameters for Particle Formation and Growth Characteristics

The growth rate of particles (GR), condensation sink (CS), condensable vapor concentration (C_v), and source rate of condensable vapor (Q) were calculated by using the size distribution of aerosol particles. Based on hourly median size distribution, in ranges of 10–25 nm, the geometric mean diameter (GMD) of particles was calculated through lognormal fitting analysis. The GR of particles was then calculated using the rate of change in the GMD (Kulmala et al., 2004). The CS, which indicates the loss rate of gaseous molecules onto pre-existing particles, was calculated using Equation 1 (Kulmala et al., 2004), taking into account the temporal evolution of the size distributions during the event. Using the estimated GR and CS values, condensable vapor concentration (C_v) and its source rate (Q) were calculated using Equations 2 and 3, assuming that the particle growth was caused by condensation of a low volatile vapor on the particle surface (Dal Maso et al., 2002; Kulmala et al., 2001):

$$\mathrm{CS} = 2\pi D_v \sum_{dp} \beta_m d_p N_{dp} \tag{1}$$

$$C_v = A \times \mathrm{GR} \tag{2}$$

$$Q = \mathrm{CS} \times C_v \tag{3}$$

where D_v is the diffusion coefficient of the condensable vapor (0.1 $\mathrm{cm^2 s^{-1}}$), β_m is the transitional regime correction factor from Fuchs and Sutugin (1971), and d_p and N_{dp} are the particle size and number concentration, respectively. A is a constant (1.37×10^7 h $\mathrm{cm^{-3}}$ $\mathrm{nm^{-1}}$) for a vapor with the molecular properties of sulfuric acid. The condensable vapor was assumed to be gaseous sulfuric acid, which reportedly plays a key role in the nucleation process (Dal Maso et al., 2005).

The hygroscopicity parameter (κ; Equation 4), and critical diameter (D_c; Equation 5) for CCN activation at a supersaturation of 0.4% were calculated using the total particle number concentrations larger than 3 nm ($\mathrm{CN_3}$), particle size distributions, and CCN concentrations as described by Furutani et al. (2008) and Petters and Kridenweis (2007):

$$\kappa = \frac{4A'^3}{27 D_c^{\,3} ln^2 SS}, \qquad A' = \frac{4\sigma_w M_w}{RT\rho_w} \tag{4}$$

$$\frac{\int_{D_0}^{D_c} n(D)dD}{N_{\mathrm{tot}}} = 1 - \frac{\mathrm{CCN}}{\mathrm{CN_3}} \tag{5}$$

where, σ_w, M_w, and ρ_w are the surface tension, molecular weight, and density of water, respectively, R is the universal gas constant, T is the temperature, SS is the supersaturation applied in the CCN counting, N_{tot} is the total number concentration of aerosol particles measured by DMPS, D is the mobility equivalent diameter, and D_o is assumed to be 10 nm, at the beginning of the DMPS scan. The κ value of ~1.4 was found to be the upper limit for the most highly CCN-active particles, such as NaCl (Petters & Kridenweis, 2007). Therefore, calculated κ values greater than 1.4 (4.4% of the data from the entire study period) were excluded. These values were possibly biased due to extremely low number concentration of aerosol particles in the pristine Arctic atmosphere.

2.4. Air Mass Transport History Analysis

The air mass back trajectories were obtained using the Hybrid Single Particle Lagrangian Integrated Trajectory model (Draxier & Hess, 1998). The model also outputs solar irradiance along the air mass back trajectory. The meteorological fields for trajectory analysis were obtained from the Global Data Assimilation System at 1° resolution. The 2-, 3-, 4-, and 5-day air mass back trajectories and hourly positions were combined with satellite-derived geographical information to evaluate the travel history of the air mass arriving at the observation site (Choi et al., 2019; E. Jang et al., 2019). Daily geographical information on sea-ice, land, and ocean area, with a 25-km resolution, was obtained from the Sea Ice Index, provided by the National Snow and Ice

Data Center. Sea surface chlorophyll concentration, a useful indicator for phytoplankton biomass, was obtained from the Level-3 product of Aqua Moderate Resolution Imaging Spectroradiometer (MODIS-Aqua) at a 4-km resolution. The air mass exposure to chlorophyll was calculated by combining 2-day air mass back trajectories and sea surface chlorophyll concentrations (Choi et al., 2019; K.-T. Park et al., 2018; Equation 6):

$$E_{\mathrm{chl}} = \frac{\sum_{t=1}^{48} \mathrm{Chl}_t}{n} \quad (6)$$

where, Chl_t is the mean sea surface chlorophyll concentration within a radius of 25 km at a given trajectory time point along the air mass back trajectory, and n is the total number of time points for which valid chlorophyll concentration is available. Here, a larger value of exposure to chlorophyll could indicate a higher possibility of the air mass carrying biologically derived compounds to the observation site.

3. Results and Discussion

3.1. Temporal Variations in Atmospheric DMS, Nanoparticles, and CCN

Atmospheric DMS mixing ratios in the Arctic atmosphere varied from 0 to >300 pptv during the phytoplankton bloom period of 2010 (Figure 1b). Temporal variations in these mixing ratios are largely controlled by meteorological parameters (e.g., air mass interaction with ocean surface and wind speed) and biological characteristics (e.g., biomass and taxonomic composition of the phytoplankton) at the observation site (K.-T. Park et al., 2013, 2018). The measured hourly number concentrations of nanoparticles range over three orders of magnitude (~10 to >10^3 cm^{-3}), and frequent NPF events were observed during the study period (Figure 1c). Both the atmospheric DMS mixing ratios and number concentrations of nanoparticles show considerable short-term (hourly to daily) variability with mean (median) values of 30.8 (4.4) ± 52.1 pptv and 234 (122) ± 313 cm^{-3}, respectively, for the study period.

The major oxidation products of DMS are sulfuric acid, hydroperoxymethyl thioformate (HPMTF), and MSA. These oxidation products can either form new particles or condense onto existing particles because of their low volatility (Chen et al., 2015; Kulmala & Kerminen, 2008; Veres et al., 2020). Since the oxidation of DMS is the only known source of MSA in the marine atmosphere, MSA concentration can be used as an indicator of DMS-derived secondary aerosol formation (Udisti et al., 2016). The MSA concentrations, measured daily, show a similar trend to the atmospheric DMS mixing ratios, with an increase starting in early May and the maximum of 200 ng m^{-3} reached when the atmospheric DMS level reached its maximum (Figure 1b).

The CCN concentrations are comparable with those reported in previous studies at other Arctic sites (J. Park et al., 2020; Schmale et al., 2018). The hourly CCN number concentration at 0.4% supersaturation varied between <10 and 400 cm^{-3} with a mean (median) of 146 (135) ± 69 cm^{-3} for the study period (Figure 1d).

3.2. Case Studies: NPF Events

To examine the correlation between biogenic DMS and aerosol properties, the NPF events were categorized into four groups: (a) high nanoparticle concentrations with low DMS mixing ratios (i.e., CN_{3-10} > 400 cm^{-3} and DMS mixing ratios <10 pptv; case A), (b) high nanoparticle concentrations with high DMS mixing ratios (i.e., CN_{3-10} > 400 cm^{-3} and DMS mixing ratios >50 pptv; case B), (c) moderate nanoparticle concentrations with high DMS mixing ratios (i.e., 150 < CN_{3-10} < 400 cm^{-3} and DMS mixing ratios >50 pptv; case C), and (d) low nanoparticle concentrations with high DMS mixing ratios (i.e., CN_{3-10} < 100 cm^{-3} and DMS mixing ratios >50 pptv; case D). Approximately 20% of the hourly DMS and nanoparticle measurements show values of >50 pptv and >400 cm^{-3}, respectively. While the time period when the hourly DMS and nanoparticles was <10 pptv and <100 cm^{-3} accounts for ~60% and 39%, respectively. Note that each case was assigned to the time periods in which the respective NPF episode lasted for >5 h (Figure 1).

The mean number concentrations of nanoparticles for cases A and B (938 ± 405 cm^{-3} and 999 ± 689 cm^{-3}, respectively) are approximately three times that of case C (309 ± 93 cm^{-3}) and more than 15 times that of case D (56 ± 31 cm^{-3}; Figure 2a). The mean DMS mixing ratios of the high DMS mixing ratio groups (i.e.,

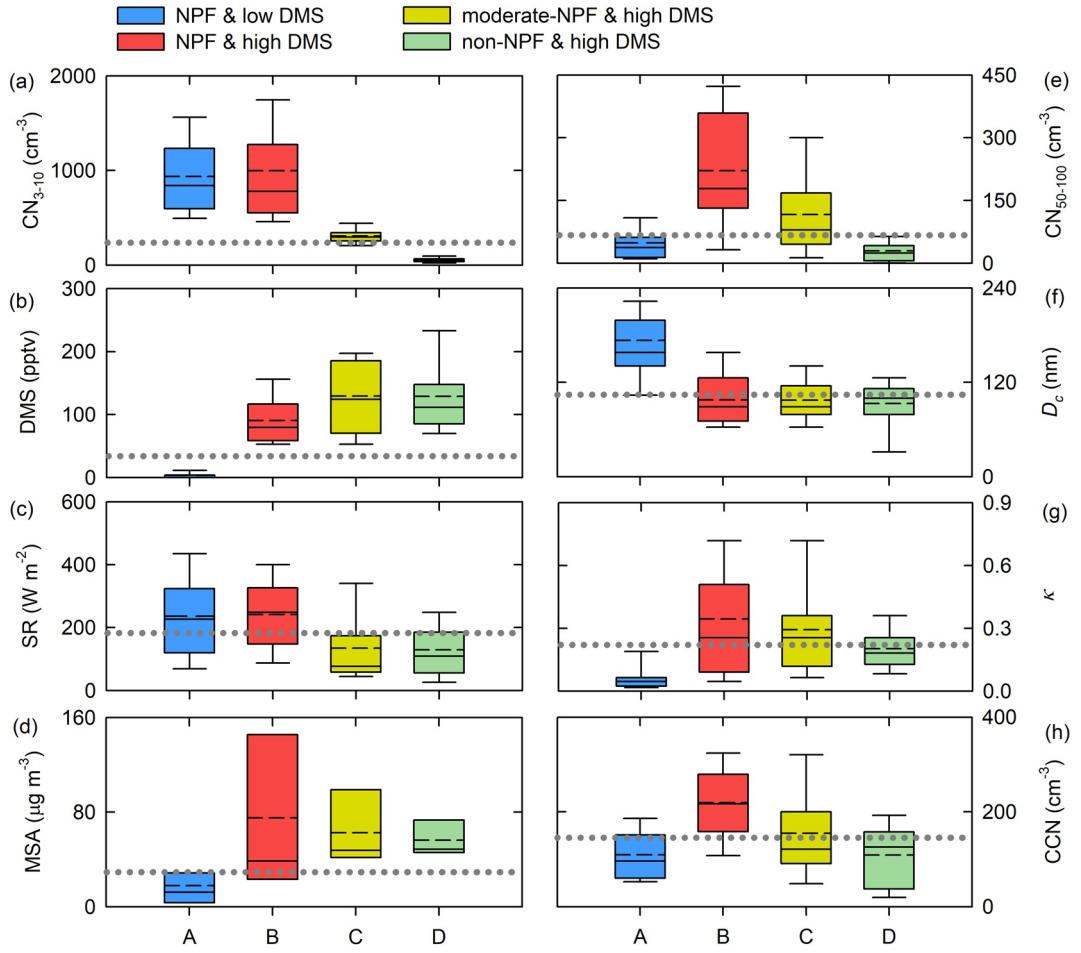

Figure 2. Box plots for (a) the number concentrations of nanoparticles ($CN_{3–10}$), (b) atmospheric dimethyl sulfide (DMS) mixing ratios, (c) solar irradiance (SR), (d) methanesulfonic acid concentrations, (e) number concentrations of Aitken mode particles ($CN_{50–100}$), (f) critical diameter for cloud condensation nuclei (CCN) activation (D_c), (g) hygroscopicity parameter (κ), and (h) number concentrations of CCN. The blue, red, yellow and green box plots indicate the results for the different NPF episodes of cases A (high new particle formation [NPF] and low DMS), B (high NPF and high DMS), C (moderate NPF and high DMS), and D (low NPF and high DMS), respectively. The gray dotted lines represent the mean values of the entire study period. The upper and lower limits of the boxes, and the solid, and the dashed lines across each box indicate the 75th and 25th percentiles, the median, and the mean, respectively.

cases B, C, and D; 90.3 ± 40.6, 129.5 ± 63.2, and 129.1 ± 58.6 pptv, respectively) are more than 30 times that of case A (2.4 ± 4.2 pptv; Figure 2b). Importantly, shipboard field measurements of DMS and particle size distribution over the Canadian Arctic Archipelago showed that DMS alone could explain the formation of newly formed particles with an initial DMS mixing ratio of ≥100 pptv in clean Arctic atmosphere (Chang et al., 2011). Among the four defined cases, case A was observed most frequently during the study period (87 h, 8 times), followed by case D (80 h, 7 times), case C (48 h, 6 times), and case B (36 h, 5 times). Cases C and D (i.e., high DMS mixing ratios but moderate and low nanoparticle concentrations) were characterized by lower solar irradiance (134 ± 110 and 129 ± 87 W m^{-2} for cases C and D, respectively) than the cases in which high concentrations of nanoparticles were observed (236 ± 136 and 242 ± 112 W m^{-2} for cases A and B, respectively; Figure 2c). This indicates that insufficient solar energy hinders the conversion of the precursor compounds (including DMS and other trace gases) into nanoparticles. Solar radiation is considered to be one of the most important factors in the occurrence of NPF events, as it is needed for the photochemical reaction that leads to the formation of sulfuric acid (Kulmala & Kerminen, 2008).

The daily MSA measurements coinciding with each one of the four cases were assigned to the cases A–D, respectively. The average MSA concentration corresponding to case B (75 ± 73 ng m^{-3}) was approximately

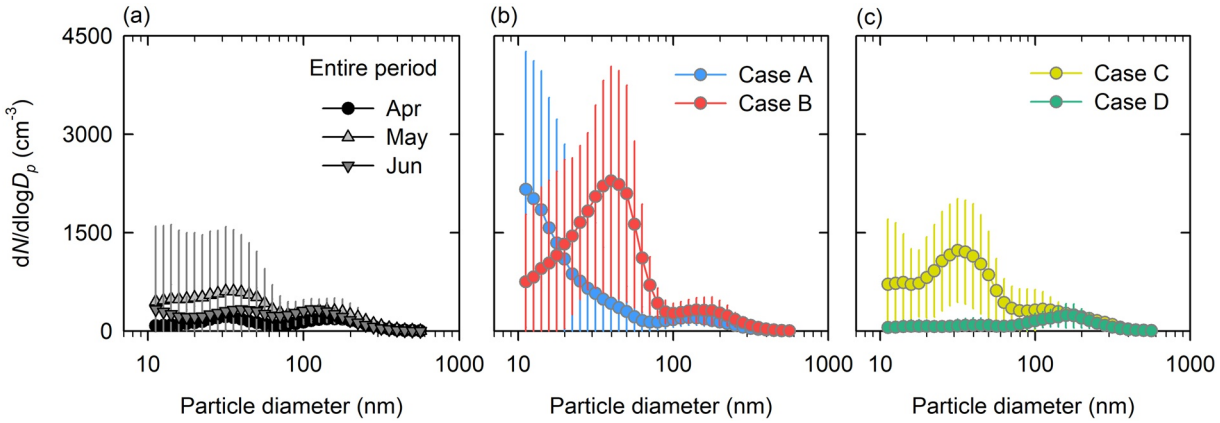

Figure 3. The size number distributions of aerosol particles ranging between 10 to 560 nm in diameter for (a) the entire study period, (b) cases A and B, and (c) cases C and D. The error bars are equivalent to 1 standard deviation (1σ).

four times that of case A (18 ± 18 ng m^{-3}), and ~20% and 30% greater than those of case C (63 ± 28 ng m^{-3}) and D (56 ± 25 ng m^{-3}), respectively (Figure 2d). Significant correlation between the MSA concentrations and both the corresponding DMS mixing ratios and the number concentrations of nanoparticles was also observed in previous study conducted in April and May 2015 at the same site (Park et al., 2017).

3.3. Case Studies: Particle Growth Events

The size distribution and chemical composition of aerosol particles are the key properties that determine the number of CCN formed at a certain water vapor supersaturation (Anttila et al., 2012; McFiggans et al., 2006). Figure 3 shows the size distribution of aerosol particles in the range of 10–560 nm, over the entire study period and for the four defined NPF cases. The number concentration of Aitken mode aerosol particles (between 50 and 100 nm in diameter; $CN_{50–100}$), which are known to be climate-relevant due to their effective growth into CCN, was four times higher for case B (221 ± 134 cm^{-3}) than for case A (49 ± 49 cm^{-3}; Figure 2e). To examine particle growth in more detail, the growth rate (GR) of particles and source rate of condensable vapor (Q) were calculated using the aerosol size distribution, regardless of the categorized NPF events. A total of 22 statistically significant particle growth events were observed during the study period (Figures S1–S4). The duration of particle growth events ranged from 7.7 to 57.0 h, with a mean of 23.0 ± 12.3 h. The growth rate of particles varied from 0.01 to 1.49 nm h^{-1} (0.62 ± 0.48 nm h^{-1}) and was comparable to the values reported in previous studies conducted in pristine polar regions (Kim et al., 2019; Weller et al., 2015). The mean atmospheric DMS mixing ratios and $CN_{3–10}$ for the 22 particle growth events were 35.9 ± 51.9 pptv and 414 ± 318 cm^{-3}, respectively.

A significant positive correlation between the average DMS mixing ratios for each particle growth event and the corresponding MSA concentrations was observed ($r = 0.89$, slope = 0.96, $n = 16$, $p < 0.01$ for the events with solar irradiance >180 W m^{-2}; $r = 0.85$, slope = 0.09, $n = 6$, $p < 0.01$ for the events with solar irradiance <180 W m^{-2}; Figure 4a). In particular, MSA-to-DMS ratio (i.e., the slope of the linear regressions), which possibly indicates the relative efficiency of DMS-to-sulfurous particle conversion, was >10 times when the solar irradiance was greater than the mean value of the entire study period (180 W m^{-2}). The source rate of condensable vapor was positively correlated with the corresponding atmospheric DMS mixing ratios ($r = 0.65$, $n = 16$, $p < 0.01$) when the solar irradiance was greater than 180 W m^{-2} (Figure 4b). A strong positive correlation was also found between the source rate of condensable vapor and the corresponding MSA concentrations for the 22 particle growth events ($r = 0.72$, $n = 22$, $p < 0.01$; Figure 4c). These support the finding that photochemical products formed from DMS were the dominant component of condensable vapor in our study area. Moreover, the increases in the growth rate of particles corresponded to a proportional increase in the DMS mixing ratios ($r = 0.64$, $n = 22$, $p < 0.01$) and the MSA concentrations ($r = 0.60$, $n = 22$, $p < 0.01$; Figure 4d).

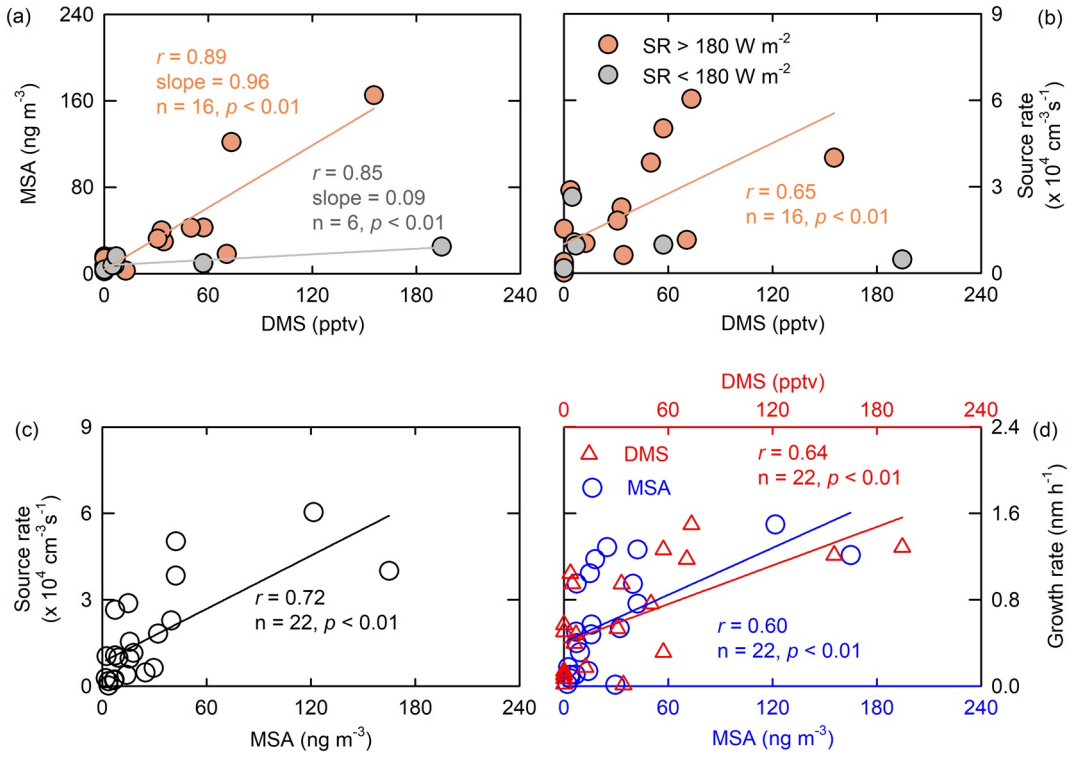

Figure 4. (a) Methanesulfonic acid (MSA) concentrations as a function of the corresponding atmospheric dimethyl sulfide (DMS) mixing ratios. (b) The source rate of condensable vapor as a function of the corresponding atmospheric DMS mixing ratios when solar irradiance is low (gray circles; <180 W m^{-2}) and high (orange circles; >180 W m^{-2}). (c) The source rate of condensable vapor as a function of MSA concentrations. (d) The growth rate of particles as a function of the corresponding atmospheric DMS mixing ratios (red triangles) and MSA concentrations (blue circles) for 22 particle growth events. The solid lines represent the best fit.

Particle growth events were further categorized into two groups: (a) particle growth with low DMS (mean DMS mixing ratio of <10 pptv during growth events, seven events, 180 h; GR-case A; Figure S1), and (b) particle growth with high DMS (mean DMS mixing ratio of >50 pptv during the growth events, five events, 135 h; GR-case B; Figure S2). The mean DMS mixing ratios for GR-case B (81.4 ± 42.6 pptv) was >100 times that of GR-case A (0.5 ± 1.4 pptv). Particle growth events that occurred under low solar radiation conditions (SR < 180 W m^{-2}, six events, 102 h; Figure S3) were excluded from the categorization to minimize the influence of meteorological factors. The average MSA concentration corresponding to GR-case B (79 ± 62 ng m^{-3}) was similar to that of case B (75 ± 73 ng m^{-3}) and was >10 times that of GR-case A (7 ± 5 ng m^{-3}; Figure 5a). The average growth rate and source rate of condensable vapor for GR-case A were estimated to be 0.35 ± 0.38 nm h^{-1} and (0.8 ± 1.0) × 10^4 cm^{-3} s^{-1}, respectively, and were <3 time that of GR-case B (1.18 ± 0.27 nm h^{-1} and (4.0 ± 1.8) × 10^4 cm^{-3} s^{-1}, respectively; Figures 5b and 5c). These results indicate that the growth of aerosol particles was more favorable for particles derived from DMS than for those derived from other potential precursors.

The potential source areas for GR-case A and GR-case B exhibited clear differences (Figures 5d–5f and Figure S5). GR-case B likely results from air mass transport over the biologically productive ocean area in the Barents and Greenland Seas. Based on a 2-day air mass transport history, the residence time of air masses over the ocean for GR-case B (27.4 ± 9.3 h) was two times that of GR-case A (12.5 ± 8.4 h; Figure 5d). Moreover, the extent of exposure of the air mass to the marine phytoplankton biomass (i.e., air mass exposure to oceanic chlorophyll; E_{chl}) for GR-case B (1.2 ± 1.0 mg m^{-3}) was six times that of GR-case A (0.2 ± 0.2 mg m^{-3}; Figure 5f). The difference in potential source origin between GR-case A and GR-case B was also notable when 3-, 4-, and 5-day air mass back trajectories were applied (Figure S5). These results strongly suggest that marine phytoplankton in the Arctic Ocean are an importance source for atmospheric DMS and DMS-derived aerosol particles (Chang et al., 2011; Heintzenberg et al., 2017; H. Lee et al., 2020;

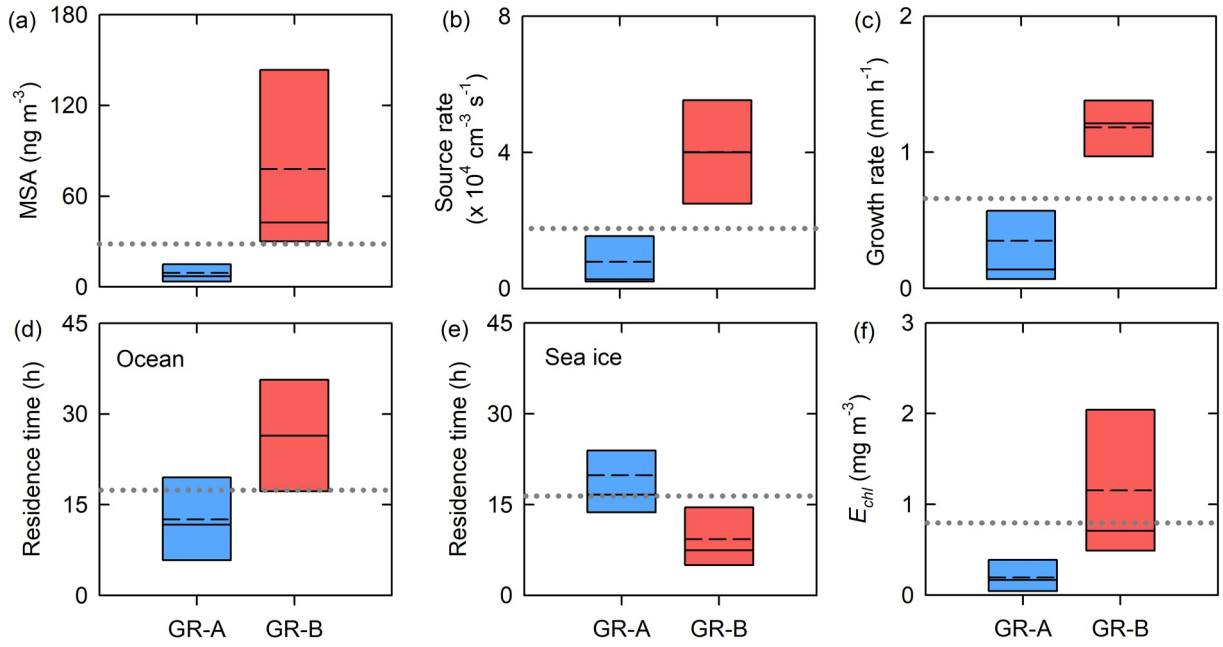

Figure 5. Box plots for (a) methanesulfonic acid concentration, (b) the source rate of condensable vapor, (c) the growth rate of particles (d), (e) residence time of 2-day air mass back trajectories arriving at the observation site over the ocean and sea-ice domain, and (f) the calculated air mass exposure to chlorophyll (E_{chl}). The blue and red box plots indicate the results for GR-case A (particle growth events with low dimethyl sulfide [DMS]) and GR-case B (particle growth events with high DMS), respectively. The gray dotted lines represent the mean values for the 22 particle growth events. The upper and lower limits of the boxes, and the solid, and the dashed lines across each box indicate the 75th and 25th percentiles, and the median, and the mean, respectively.

K.-T. Park et al., 2017). During GR-case A, air masses spent more time over the sea-ice covered region (19.8 ± 9.7 h) than during GR-case B (8.9 ± 6.9 h; Figure 5e). Recent studies reported that abiotic and biotic release of iodine-containing particles from sea-ice could also be contributing to the formation of newly formed particles in the Arctic and Antarctic atmosphere (Allan et al., 2015; Raso et al., 2017; Sipilä et al., 2016). Although iodine compounds were not measured during the study period, key precursor compounds that are associated with particle formation and growth during GR-case A were probably derived from iodine compounds recently released from ice-covered areas.

3.4. Linking DMS-Derived Particle to CCN

A previous study performed at the same observation site reported a range in annual median CCN concentrations of 45–81 cm^{-3} at a supersaturation of 0.4% throughout 7 years long (from 2007 to 2013) in situ CCN observation campaign (Jung et al., 2018). The highest CCN concentration was recorded in March (~150 cm^{-3}), mostly due to high loading of anthropogenic accumulation mode particles (>100 nm in diameter) transported from mid-latitude regions, known as Arctic haze (Quinn et al., 2007). A sharp transition in the dominant particle type (large to small particles) was identified in springtime, owing to a weakening of Arctic haze events and increasing biogenic production in the Arctic Ocean (Engvall et al., 2008). As the condensation sink is proportional to the surface area of existing particles, the resulting reduction in the condensation sink could promote NPF in clean Arctic atmosphere (Leaitch et al., 2013). Following the Arctic haze period, the anthropogenic influence on aerosol properties rapidly decreased and remained low until late winter. However, CCN concentrations during May and June remained high, possibly due to the supply of newly formed particles originating from biogenic sources (Jung et al., 2018; Leaitch et al., 2013).

To examine the hygroscopic properties of aerosol particles, we calculated the hygroscopicity parameter (κ) and critical diameter (D_c) for CCN activation at a supersaturation of 0.4%. In general, κ values are zero for non-hygroscopic compounds, and between 0.01 and 0.5 for slightly-to very-hygroscopic organic species (Petters & Kreidenweis, 2007). The mean κ value of the entire study period is 0.23 ± 0.19, which is comparable to the results of previous studies from Arctic areas. For example, κ values between 0.11 and 0.41

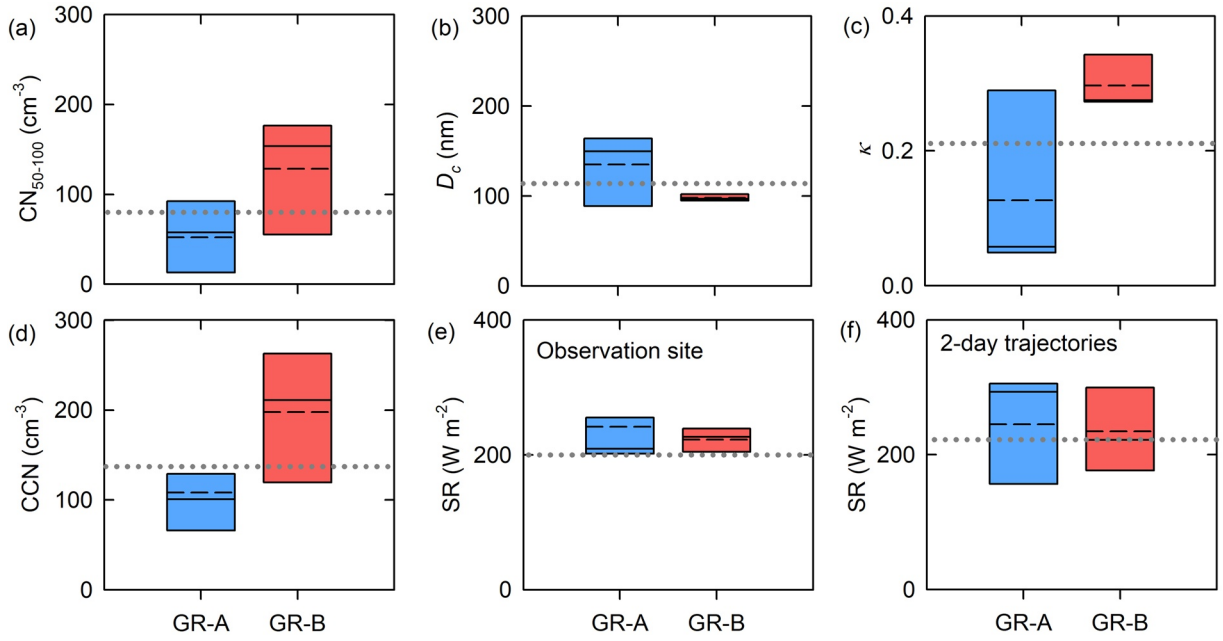

Figure 6. Box plot for (a) the number concentration of Aitken mode particles ($CN_{50–100}$), (b) critical diameter for cloud condensation nuclei (CCN) activation (D_c), (c) hygroscopicity parameter (κ), (d) number concentrations of CCN, (e) solar irradiance (SR) measured at the observation site, and (f) SR averaged along 2-day air mass back trajectories. The blue and red box plots indicate the results for the different particle growth episodes, including GR-case A (particle growth events with low dimethyl sulfide [DMS]) and GR-case B (particle growth events with high DMS), respectively. The gray dotted lines represent the mean values for 22 particle growth events. The upper and lower limits of the boxes, and the solid and dashed lines across each box indicate the 75th and 25th percentiles, and the median and mean, respectively.

were estimated during an Arctic expedition near the Svalbard archipelago in the spring-summer period of 2017 (Kecorius et al., 2019). Variations in the D_c may reflect alterations in the chemical composition of the aerosol particles. Thus, as the hygroscopicity of the aerosol increases, the D_c for CCN activation decreases (Sihto et al., 2011). The D_c for aerosols allocated to the three NPF cases with high DMS is similar (98 ± 35, 97 ± 29, and 93 ± 35 nm for cases B, C, and D, respectively) and approximately 70% lower than that of case A (163 ± 70 nm; Figure 2f). Furthermore, the mean κ value for case B (0.34 ± 0.26) is four times greater than that of case A (0.08 ± 0.11; Figure 2g). These results indicate that the aerosol particles observed during the periods of DMS-derived formation and growth of aerosol particles contain a larger number of hygroscopic compounds. Consequently, the mean number concentration of CCN at 0.4% supersaturation for case B (219 ± 81 cm^{-3}) is 50% greater than the mean CCN concentration of the entire study period (146 ± 69 cm^{-3}) and twice that of case A (110 ± 48 cm^{-3}; Figure 2h), although the number concentration of nanoparticles is similar (938 ± 405 cm^{-3} and 999 ± 689 cm^{-3} for cases A and B, respectively; Figure 2a). Such remarkable differences in the number concentration of Aitken mode particles, D_c, κ values, and CCN concentrations were also found between episodes of GR-case A and GR-case B, although the intensify of solar irradiance (both measured at the observation site and averaged along 2-day air mass back trajectories) was similar (Figures 6a–6f). Explicitly, D_c for GR-case B (98 ± 4 nm) was approximately 40% lower than that of GR-case A (135 ± 34 nm). The number concentration of Aitken mode particles, κ value, and CCN concentration for GR-case B (128 ± 71 cm^{-3}, 0.30 ± 0.04, and 198 ± 77 cm^{-3}, respectively) were approximately twice those of GR-case A (52 ± 37 cm^{-3}, 0.13 ± 0.12, and 108 ± 46 cm^{-3}, respectively). These results suggest that the formation of new DMS-derived particles could effectively contribute to the growth of particles to a climate-relevant size and the activation of CCN in the Arctic atmosphere.

Additionally, the diurnal cycles of solar irradiance, DMS mixing ratios, $CN_{3–10}$, $CN_{10–20}$, $CN_{50–100}$, and CCN were examined for the selected particle growth events of GR-case A and GR-case B (Figure 7). The diurnal patterns of solar irradiance for GR-cases A and B were comparable and peaked around noon local time (Figure 7a). In both cases, the increasing pattern of $CN_{3–10}$ and $CN_{10–20}$ lagged a few hours behind the increase in solar irradiance (Figures 7c and 7d). This phenomenon could indicate that the observed NPF events started

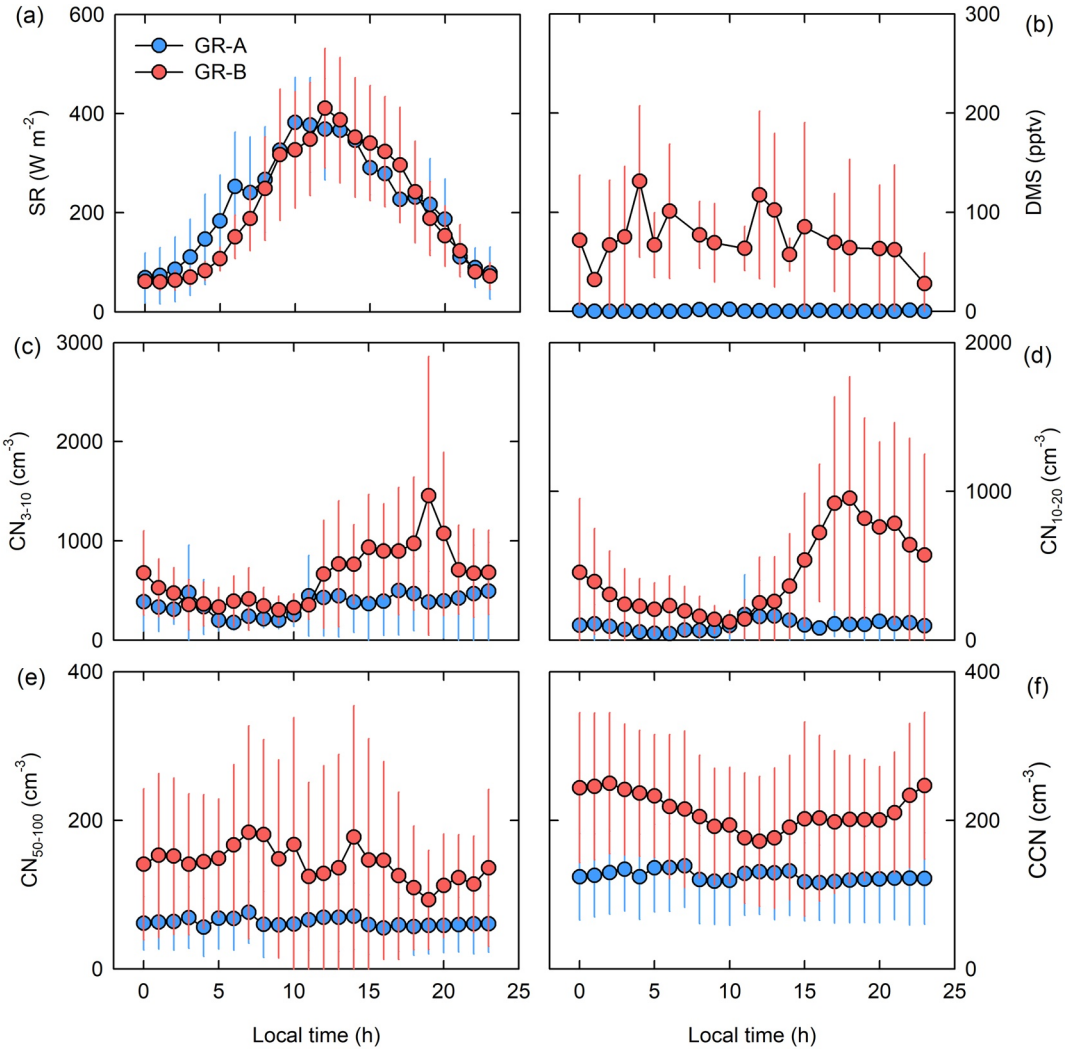

Figure 7. Diurnal cycles of (a) solar irradiance, (b) atmospheric DMS mixing ratios, the number concentrations of (c) nanoparticles ($CN_{3–10}$), (d) particles with diameters between 10 and 20 nm (CN10–20), (e) Aitken mode particles ($CN_{50–100}$), and cloud condensation nuclei. The error bars are equivalent to 1 standard deviation (1σ). The blue and red circles indicate the results for the episodes of GR-case A (particle growth with low dimethyl sulfide [DMS]) and GR-case B (particle growth with high DMS), respectively.

to occur dozens to hundreds of kilometers from the observation site (i.e., not freshly nucleated particles; Zheng et al., 2021). Importantly, the increase rate of the number concentration of particles smaller than 20 nm appeared to be more notable for GR-case B than for GR-case A.

4. Conclusions and Implication

Several long-term observation studies and shipboard campaign have shown a strong seasonal coupling between biogenic sulfur compounds (including DMS, MSA, and non-sea-salt sulfate), and CCN (Andreae et al., 1995; Ayers & Gras, 1991; Ayers et al., 1997; Gras & Keywood, 2017; Leaitch et al., 2013; Sanchez et al., 2018). However, such a coherence in seasonality could not provide applicable evidence to clearly support the DMS-derived formation of climate-relevant particles and CCN in marine atmospheres (Quinn & Bates, 2011). This is due to several biogenic volatile compounds and organics being able to influence the enhancement of marine aerosols and CCN during the productive periods (Bigg, 2007; Rinaldi et al., 2010). Moreover, DMS in the atmosphere is a short-lived species with a half-life of less than two days (Barnes et al., 2006), and the growth of newly formed particles with sizes of up to a few tens of nanometers can

be completed within a few hours (Kerminen et al., 2018). Recently, HPMTF was identified as one of the major oxidative products of biogenic DMS (Veres et al., 2020). Thus, additional studies determining the atmospheric fate of HPMTF (e.g., oxidation process, spatial and temporal variations, and association with NPF and particle growth) are needed to assess the role of DMS in marine sulfur chemistry. To this end, simultaneous high-frequency measurements of diverse physiochemical parameters are required to obtain observational evidence for the DMS-induced enhancement of marine CCN.

There has been increasing attention on understanding Arctic aerosols because warming-induced changes in Arctic ecosystem could seriously affect primary and secondary organic aerosol formation processes that related to climate forcing (Abbatt et al., 2019). Biogenic DMS emission is of interest due to its potential contribution to the formation of climate relevant particles in Arctic atmosphere. We evaluated and presented convincing linkage within the phytoplankton-DMS-aerosol-CCN system by analyzing the detailed particle formation and growth-related parameters, as well as the potential source origin in the pristine Arctic atmosphere. Although our field observations did not consider the time delay between gaseous precursors, particle nucleation, and initial growth steps, this case study shows that the DMS-derived formation and growth of aerosol particles was accompanied by a significant increase in climate-relevant particles, which were are also more suitable to act as CCN due to their higher hygroscopicity. According to ground-based and shipboard measurements of atmospheric DMS and MSA over the Arctic and Antarctic oceans, high levels of DMS (>100 pptv) and MSA (>70 ng m^{-3}) were frequently observed during the biologically productive periods (Berresheim et al., 1998; Marandino et al., 2008; Mungall et al., 2016; Preunkert et al., 2007; Read et al., 2008; Staubes & Georgii, 1993; Zhang et al., 2020). These observations possibly indicate that DMS-induced enhancement of aerosols and CCN formation is a widespread phenomenon in Arctic and Antarctic regions where phytoplankton producing DMS are abundant (i.e., a sufficient source of condensable vapor), but background particle concentrations are low (i.e., low condensation sinks). Considering that the increasing production of DMS associated with sea ice decreases as a result of global warming (Galí et al., 2019; Sharma et al., 2012), the contribution of DMS to CCN formation will increase in the foreseeable future.

Although relationships with other key precursors such as halogenated gases, and N-containing organics, which may have contributed to these processes, have not yet been explored, our results provide robust observational evidence supporting a close interaction between DMS, aerosols, and CCN in the Arctic atmosphere. To confirm the roles of biogenic DMS in climate feedback, long-term and simultaneous observations of key gaseous precursors and physiochemical properties of aerosol particles are critical, along with the improvement of model prediction of the association of planktonic DMS, aerosols, and climate.

Data Availability Statement

Data for aerosol properties measured using CCNC, CPC, and DMPS at Zeppelin observatory can be accessed from the EBAS database (http://ebas.nilu.no/default.aspx). Solar irradiance data were provided by the Alfred Wegener Institute, Helmholtz Centre for Polar and Marine Research (https://doi.org/10.1594/PANGAEA.873812).

Acknowledgments
This study has been supported by the National Research Foundation of Korea (grant nos. NRF-2021M1A5A1065425 (KOPRI-PN21011) and NRF-2021R1A2C3008748).

References

Abbatt, J. P. D., Leaitch, W. R., Aliabadi, A. A., Bertram, A. K., Blanchet, J., Boivin-Rioux, A., et al. (2019). Overview paper: New insights into aerosol and climate in the Arctic. *Atmospheric Chemistry and Physics*, *19*, 2527–2560. https://doi.org/10.5194/acp-19-2527-2019

Allan, J. D., Williams, P. I., Najera, J., Whitehead, J. D., Flynn, M. J., Taylor, J. W., et al. (2015). Iodine observed in new particle formation events in the Arctic atmosphere during ACCACIA. *Atmospheric Chemistry and Physics*, *15*, 5599–5609. https://doi.org/10.5194/acp-15-5599-2015

Andreae, M. O., Elbert, W., & de Mora, S. J. (1995). Biogenic sulfur emissions and aerosols over the tropical South Atlantic. 3. Atmospheric dimethylsulfide, aerosols and cloud condensation nuclei. *Journal of Geophysical Research*, *100*, 11335–11356. https://doi.org/10.1029/94JD02828

Anttila, T., Brus, D., Jaatinen, A., Hyvärinen, A.-P., Kivekäs, N., Romakkaniemi, S., et al. (2012). Relationships between particles, cloud condensation nuclei and cloud droplet activation during the third Pallas Cloud Experiment. *Atmospheric Chemistry and Physics*, *12*, 11435–11450. https://doi.org/10.5194/acp-12-11435-2012

Ayers, G. P., & Cainey, J. M. (2007). The CLAW hypothesis: A review of the major developments. *Environmental Chemistry*, *4*, 366–374. https://doi.org/10.1071/EN07080

Ayers, G. P., Cainey, J. M., Gillett, R. W., & Ivey, J. P. (1997). Atmospheric sulphur and cloud condensation nuclei in marine air in the southern hemisphere. *Philosophical Transactions of the Royal Society B*, *352*, 203–211. https://doi.org/10.1098/rstb.1997.0015

Ayers, G. P., & Gras, J. L. (1991). Seasonal relationship between cloud condensation nuclei and aerosol methanesulfonate in marine air. *Nature*, *353*, 834–835. https://doi.org/10.1038/353834a0

Barnes, I., Hjorth, J., & Mihalopoulos, N. (2006). Dimethyl sulfide and dimethyl sulfoxide and their oxidation in the atmosphere. *Chemical Reviews*, *106*, 940–975. https://doi.org/10.1021/cr020529+

Becagli, S., Lazzara, L., Marchese, C., Dayan, U., Ascanius, S. E., Cacciani, M., et al. (2016). Relationships linking primary production, sea ice melting, and biogenic aerosol in the Arctic. *Atmospheric Environment*, *136*, 1–15. https://doi.org/10.1016/j.atmosenv.2016.04.002

Berresheim, H., Huey, J. W., Thorn, R. P., Eisele, F. L., Tanner, D. J., & Jefferson, A. (1998). Measurements of dimethyl sulfide, dimethyl sulfoxide, dimethyl sulfone, and aerosol ions at Palmer Station, Antarctica. *Journal of Geophysical Research*, *103*, 1629–1637. https://doi.org/10.1029/97JD00695

Bigg, E. K. (2007). Sources, nature, and influence on climate of marine airborne particulates. *Environmental Chemistry*, *4*, 155–161. https://doi.org/10.1071/EN07001

Boy, M., Kulmala, M., Ruuskanen, T. M., Pihlatie, M., Reissell, A., Aalto, P. P., et al. (2005). Sulphuric acid closure and contribution to nucleation mode particle growth. *Atmospheric Chemistry and Physics*, *5*, 863–878. https://doi.org/10.5194/acp-5-863-2005

Brooks, S. D., & Thornton, D. C. O. (2018). Marine Aerosols and Clouds. *Annual Review of Marine Science*, *10*, 289–313. https://doi.org/10.1146/annurev-marine-121916-063148

Carslaw, K., Lee, S. L., Reddington, A., Pringle, C. L., Rap, K. J., Forster, A., et al. (2013). Large contribution of natural aerosols to uncertainty in indirect forcing. *Nature*, *503*, 67–71. https://doi.org/10.1038/nature12674

Chang, R. Y.-W., Sjostedt, S. J., Pierce, J. R., Papakyriakou, T. N., Scarratt, M. G., Michaud, S., et al. (2011). Relating atmospheric and oceanic DMS levels to particle nucleation events in the Canadian Arctic Summer. *Journal of Geophysical Research*, *116*, D00S03. https://doi.org/10.1029/2011JD015926

Charlson, R. J., Lovelock, J. E., Andreae, M. O., & Warren, S. G. (1987). Oceanic phytoplankton, atmospheric sulphur, cloud albedo and climate. *Nature*, *326*, 655–661. https://doi.org/10.1038/326655a0

Chen, H., Ezell, M. J., Arquero, K. D., Varner, M. E., Dawson, M. L., Gerber, R. B., & Finlayson-Pitts, B. J. (2015). New particle formation and growth from methanesulfonic acid, trimethylamine and water. *Physical Chemistry Chemical Physics*, *17*, 13699–13709. https://doi.org/10.1039/C5CP00838G

Choi, J. H., Jang, E., Yoon, Y. J., Park, J. Y., Kim, T.-W., Becagli, S., et al. (2019). Influence of biogenic organics on the chemical composition of Arctic aerosols. *Global Biogeochemical Cycles*, *33*, 1238–1250. https://doi.org/10.1029/2019GB006226

Dal Maso, M., Kulmala, M., Lehtinen, K. E. J., Mäkelä, J. M., Aalto, P., & O'Dowd, C. D. (2002). Condensation and coagulation sinks and formation of nucleation mode particles in coastal and boreal forest boundary layers. *Journal of Geophysical Research*, *107*(D19). https://doi.org/10.1029/2001JD001053

Dal Maso, M., Kulmala, M., Riipinen, I., Wagner, R., Hussein, T., Aalto, P. P., & Lehtinen, K. E. J. (2005). Formation and growth of fresh atmospheric aerosols: Eight years of aerosol size distribution data from SMEAR II, Hyytiälä, Finland. *Boreal Environment Research*, *10*(5), 323–336.

Draxier, R. R., & Hess, G. D. (1998). An overview of the HYSPLIT_4 modeling system for trajectories, dispersion and deposition. *Australian Meteorological Magazine*, *47*, 295–308.

Engvall, A.-C., Krejci, R., Ström, J., Treffeisen, R., Scheele, R., Hermansen, O., & Paatero, J. (2008). Changes in aerosol properties during spring-summer period in the Arctic troposphere. *Atmospheric Chemistry and Physics*, *8*, 445–462. https://doi.org/10.5194/acp-8-445-2008

Fuchs, N. A., & Sutugin, A. G. (1971). Highly dispersed aerosols. In G. M. Hidy, & J. R. Brock (Eds.), *Topics in Current Aerosol Research*. Pergamon.

Furutani, H., Dall'osto, M., Roberts, G. C., & Prather, K. A. (2008). Assessment of the relative importance of atmospheric aging on CCN activity derived from field observations. *Atmospheric Environment*, *42*, 3130–3142. https://doi.org/10.1016/j.atmosenv.2007.09.024

Galí, M., Devred, E., Babin, M., & Levasseur, M. (2019). Decadal increase in Arctic dimethylsulfide emission. *Proceedings of the National Academy of Sciences of the United States of America*, *116*, 19311–19317. https://doi.org/10.1073/pnas.1904378116

Gras, J. L., & Keywood, M. (2017). Cloud condensation nuclei over the Southern Ocean: Wind dependence and seasonal cycles. *Atmospheric Chemistry and Physics*, *17*, 4419–4432. https://doi.org/10.5194/acp-17-4419-2017

Heintzenberg, J., Tunved, P., Gali, M., & Leck, C. (2017). New particle formation in the Svalbard region 2006–2015. *Atmospheric Chemistry and Physics*, *17*, 6153–6175. https://doi.org/10.5194/acp-17-6153-2017

Hopkins, F. E., Suntharalingam, P., Gehlen, M., Andrews, O., Archer, S. D., Bopp, L., et al. (2020). The impacts of ocean acidification on marine trace gases and the implications for atmospheric chemistry and climate. *Proceedings of the Royal Society A: Mathematical, Physical & Engineering Sciences*, *476*(2237), 20190769. https://doi.org/10.1098/rspa.2019.0769

Jang, E., Park, K. T., Yoon, Y. J., Kim, T. W., Hong, S. B., Becagli, S., et al. (2019). New particle formation events observed at the King Sejong Station, Antarctic Peninsula – Part 2: Link with the oceanic biological activities. *Atmospheric Chemistry and Physics*, *19*, 7595–7608. https://doi.org/10.5194/acp-19-7595-2019

Jang, S., Park, K.-T., Lee, K., & Suh, Y.-S. (2016). An analytical system enabling consistent and long-term measurement of atmospheric dimethyl sulfide. *Atmospheric Environment*, *134*, 217–223. https://doi.org/10.1016/j.atmosenv.2016.03.041

Jung, C. H., Yoon, Y. J., Kang, H. J., Gim, Y., Lee, B. Y., Ström, J., et al. (2018). The seasonal characteristics of cloud condensation nuclei (CCN) in the arctic lower troposphere. *Tellus B: Chemical and Physical Meteorology*, *70*, 1–13. https://doi.org/10.1080/16000889.2018.1513291

Kecorius, S., Vogl, T., Paasonen, P., Lampilahti, J., Rothenberg, D., Wex, H., et al. (2019). New particle formation and its effect on cloud condensation nuclei abundance in the summer Arctic: A case study in the Fram Strait and Barents Sea. *Atmospheric Chemistry and Physics*, *19*, 14339–14364. https://doi.org/10.5194/acp-19-14339-2019

Kerminen, V. M., Chen, X., Vakkari, V., Petäjä, T., Kulmala, M., & Bianchi, F. (2018). Atmospheric new particle formation and growth: Review of field observations. *Environmental Research Letters*, *13*, 10. https://doi.org/10.1088/1748-9326/aadf3c

Kettle, A. J., Andreae, M. O., Amouroux, D., Andreae, T. W., Bates, T. S., Berresheim, H., et al. (1999). A global database of sea surface dimethylsulfide (DMS) measurements and a procedure to predict sea surface DMS as a function of latitude, longitude, and month. *Global Biogeochemical Cycles*, *13*(2), 399–444. https://doi.org/10.1029/1999GB900004

Kim, J., Yoon, Y. J., Gim, Y., Choi, J. H., Kang, H. J., Park, K.-T., et al. (2019). New particle formation events observed at King Sejong Station, Antarctic Peninsula – Part 1: Physical characteristics and contribution to cloud condensation nuclei. *Atmospheric Chemistry and Physics*, *19*, 7583–7594. https://doi.org/10.5194/acp-19-7583-2019

Kulmala, M. (2003). How particles nucleate and grow. *Science*, *302*, 1000–1001. https://doi.org/10.1126/science.1090848

Kulmala, M., Dal Maso, M., Mäkelä, J. M., Pirjola, L., Väkevä, M., Aalto, P., et al. (2001). On the formation, growth and composition of nucleation mode particles. *Tellus B: Chemical and Physical Meteorology*, *53*(4), 479–490. https://doi.org/10.3402/tellusb.v53i4.16622

Kulmala, M., & Kerminen, V. M. (2008). On the formation and growth of atmospheric nanoparticles. *Atmospheric Research*, *90*(2–4), 132–150. https://doi.org/10.1016/j.atmosres.2008.01.005

Kulmala, M., Vehkamaki, H., Petajda, T., Dal Maso, M., Lauri, A., Kerminen, V. M., et al. (2004). Formation and growth rates of ultrafine atmospheric particles: A review of observations. *Journal of Aerosol Science*, *35*, 143–176. https://doi.org/10.1016/j.jaerosci.2003.10.003

Lana, A., Bell, T. G., Simó, R., Vallina, S. M., Ballabrera-Poy, j., Kettel, A. J., et al. (2011). An updated climatology of surface dimethylsulfide concentrations and emission fluxes in the global ocean. *Global Biogeochemical Cycles*, GB1004. https://doi.org/10.1029/2010gb003850

Leaitch, W. R., Sharma, S., Huang, L., Toom-Sauntry, D., Chivulescu, A., Macdonald, A. M., et al. (2013). Dimethyl sulfide control of the clean summertime Arctic aerosol and cloud. *Elementa: Science of the Anthropocene*, *1*, 000017. https://doi.org/10.12952/journal.elementa.000017

Lee, H., Lee, K., Lunder, C. R., Krejci, R., Aas, W., Park, J., et al. (2020). Atmospheric new particle formation characteristics in the Arctic as measured at Mount Zeppelin, Svalbard, from 2016 to 2018. *Atmospheric Chemistry and Physics*, *20*, 13425–13441. https://doi.org/10.5194/acp-20-13425-2020

Lee, K., Sabine, C. L., Tanhua, T., Kim, T.-W., Feely, R. A., & Kim, H.-C. (2011). Roles of marginal seas in absorbing and storing fossil fuel CO_2. *Energy & Environmental Science*, *4*(4), 1133–1146. https://doi.org/10.1039/C0EE00663G

Lee, S.-H., Gordon, H., Yu, H., Lehtipalo, K., Haley, R., Li, Y., & Zhang, R. (2019). New particle formation in the atmosphere: From molecular clusters to global climate. *Journal of Geophysical Research: Atmospheres*, *124*, 7098–7146. https://doi.org/10.1029/2018JD029356

Levasseur, M. (2013). Impact of Arctic meltdown on the microbial cycling of sulphur. *Nature Geoscience*, *6*, 691–700. https://doi.org/10.1038/ngeo1910

Marandino, C. A., De Bruyn, W. J., Miller, S. D., & Saltzman, E. S. (2008). DMS air/sea flux and gas transfer coefficients from the North Atlantic summertime coccolithophore bloom. *Geophysical Research Letters*, *35*, L23812. https://doi.org/10.1029/2008GL036370

McFiggans, G., Artaxo, P., Baltensperger, U., Coe, H., Facchini, M. C., Feingold, G., et al. (2006). The effect of physical and chemical aerosol properties on warm cloud droplet activation. *Atmospheric Chemistry and Physics*, *6*, 2593–2649. https://doi.org/10.5194/acp-6-2593-2006

Mungall, E. L., Croft, B., Lizotte, M., Thomas, J. L., Murphy, J. G., Levasseur, M., et al. (2016). Dimethyl sulfide in the summertime Arctic atmosphere: Measurements and source sensitivity simulations. *Atmospheric Chemistry and Physics*, *16*, 6665–6680. https://doi.org/10.5194/acp-16-6665-2016

O'Dowd, C. D., & De Leeuw, G. (2007). Marine aerosol production: A review of the current knowledge. *Philosophical Transactions of the Royal Society A*, *365*, 1753–1774. https://doi.org/10.1098/rsta.2007.2043

Park, J., Dall'Osto, M., Park, K., Gim, Y., Kang, H. J., Jang, E., et al. (2020). Shipborne observations reveal contrasting Arctic marine, Arctic terrestrial and Pacific marine aerosol properties. *Atmospheric Chemistry and Physics*, *20*, 5573–5590. https://doi.org/10.5194/acp-20-5573-2020

Park, K.-T., Jang, S., Lee, K., Yoon, Y. J., Kim, M.-S., Park, K., et al. (2017). Observational evidence for the formation of DMS-derived aerosols during Arctic phytoplankton blooms. *Atmospheric Chemistry and Physics*, *17*, 9665–9675. https://doi.org/10.5194/acp-17-9665-2017

Park, K.-T., Lee, K., Kim, T. W., Yoon, Y. J., Jang, E. H., Jang, S., et al. (2018). Atmospheric DMS in the Arctic Ocean and its relation to phytoplankton biomass. *Global Biogeochemical Cycles*, *32*, 351–359. https://doi.org/10.1002/2017GB005805

Park, K.-T., Lee, K., Shin, K., Jeong, H. J., & Kim, K. Y. (2014). Improved method for minimizing sulfur loss in analysis of particulate organic sulfur. *Analytical Chemistry*, *86*, 1352–1356. https://doi.org/10.1021/ac403649m

Park, K.-T., Lee, K., Yoon, Y. J., Lee, H. W., Kim, H. C., Lee, B. Y., et al. (2013). Linking atmospheric dimethyl sulfide and the Arctic Ocean spring bloom. *Geophysical Research Letters*, *40*, 155–160. https://doi.org/10.1029/2012GL054560

Petters, M. D., & Kreidenweis, S. M. (2007). A single parameter representation of hygroscopic growth and cloud condensation nucleus activity. *Atmospheric Chemistry and Physics*, *7*, 1961–1971. https://doi.org/10.5194/acp-7-1961-2007

Preunkert, S., Legrand, M., Jourdain, B., Moulin, C., Belviso, S., Kasamatsu, N., et al. (2007). Interannual variability of dimethylsulfide in air and seawater and its atmospheric oxidation by-products (methanesulfonate and sulfate) at Dumont d'Urville, coastal Antarctica (1999–2003). *Journal of Geophysical Research: Atmosphere*, *112*, D06306. https://doi.org/10.1029/2006JD007585

Quinn, P. K., & Bates, T. S. (2011). The case against climate regulation via oceanic phytoplankton sulphur emissions. *Nature*, *480*, 51–56. https://doi.org/10.1038/nature10580

Quinn, P. K., Shaw, G., Andrews, E., Dutton, E. G., Ruoho-Airola, T., & Gong, S. L. (2007). Arctic haze: Current trends and knowledge gaps. *Tellus B: Chemical and Physical Meteorology*, *59*, 99–114. https://doi.org/10.1111/j.1600-0889.2006.00238.x10.1111/j.1600-0889.2006.00236.x

Raso, A. R. W., Custard, K. D., May, N. W., Tanner, D., Newburn, M. K., Walker, L., et al. (2017). Active molecular iodine photochemistry in the Arctic. *Proceedings of the National Academy of Sciences of the United States of America*, *114*(38), 10053–10058. https://doi.org/10.1073/pnas.1702803114

Read, K. A., Lewis, A. C., Bauguitte, S., Rankin, A. M., Salmon, R. A., Wolff, E. W., et al. (2008). DMS and MSA measurements in the Antarctic Boundary Layer: Impact of BrO on MSA production. *Atmospheric Chemistry and Physics*, *8*, 2985–2997. https://doi.org/10.5194/acp-8-2985-2008

Rinaldi, M., Decesari, S., Finessi, E., Giulianelli, L., Carbone, C., Fuzzi, S., et al. (2010). Primary and secondary organic marine aerosol and oceanic biological activity: Recent results and new perspectives for future studies. *Advances in Meteorology*, 1–10. https://doi.org/10.1155/2010/310682

Sanchez, K. J., Chen, C. L., Russell, L. M., Betha, R., Liu, J., Price, D. J., et al. (2018). Substantial seasonal contribution of observed biogenic sulfate particles to cloud condensation nuclei. *Scientific Reports*, *8*, 3235. https://doi.org/10.1038/s41598-018-21590-9

Schmale, J., Henning, S., Decesari, S., Henzing, B., Keskinen, H., Sellegri, K., et al. (2018). Long-term cloud condensation nuclei number concentration, particle number size distribution and chemical composition measurements at regionally representative observatories. *Atmospheric Chemistry and Physics*, *18*, 2853–2881. https://doi.org/10.5194/acp-18-2853-2018

Sharma, S., Chan, E., Ishizawa, M., Toom-Sauntry, D., Gong, S. L., Li, S. M., et al. (2012). Influence of transport and ocean ice extent on biogenic aerosol sulfur in the Arctic atmosphere. *Journal of Geophysical Research: Atmosphere*, *117*, D12209. https://doi.org/10.1029/2011JD017074

Sihto, S.-L., Mikkilä, J., Vanhanen, J., Ehn, M., Liao, L., Lehtipalo, K., et al. (2011). Seasonal variation of CCN concentrations and aerosol activation properties in boreal forest. *Atmospheric Chemistry and Physics*, *11*, 13269–13285. https://doi.org/10.5194/acp-11-13269-2011

Simó, R. (2001). Production of atmospheric sulfur by oceanic plankton: Biogeochemical, ecological and evolutionary links. *Trends in Ecology & Evolution*, *16*, 287–294. https://doi.org/10.1016/s0169-5347(01)02152-8

Sipilä, M., Sarnela, N., Jokinen, T., Henschel, H., Junninen, H., Kontkanen, J., et al. (2016). Molecular-scale evidence of aerosol particle formation via sequential addition of HIO_3. *Nature*, *537*, 532–534. https://doi.org/10.1038/nature19314

Staubes, R., & Georgii, H.-W. (1993). Biogenic sulfur compounds in seawater and the atmosphere of the Antarctic region. *Tellus B: Chemical and Physical Meteorology*, *45*, 127–137. https://doi.org/10.3402/tellusb.v45i2.15587

Stroeve, J., Holland, M. M., Meier, W., Scambos, T., & Serreze, M. (2007). Arctic sea ice decline: Faster than forecast. *Geophysical Research Letters*, *34*, L09501. https://doi.org/10.1029/2007GL029703

Udisti, R., Bazzano, A., Becagli, S., Bolzacchini, E., Caiazzo, L., Cappelletti, D., et al. (2016). Sulfate source apportionment in the Ny-Ålesund (Svalbard Islands) Arctic aerosol. *Rendiconti Lincei. Scienze Fisiche e Naturali*, *27*, 85–94. https://doi.org/10.1007/s12210-016-0517-7

Veres, P. R., Neuman, J. A., Bertram, T. H., Assaf, E., Wolfe, G. M., Williamson, C. J., et al. (2020). Global airborne sampling reveals a previously unobserved dimethyl sulfide oxidation mechanism in the marine atmosphere. *Proceedings of the National Academy of Sciences of the United States of America*, *117*, 4505–4510. https://doi.org/10.1073/pnas.1919344117

Wang, S., Maltrud, M. E., Burrows, S. M., Elliott, S. M., & Cameron-Smith, P. (2018). Impacts of shifts in phytoplankton community on clouds and climate via the sulfur cycle. *Global Biogeochemical Cycles*, *32*, 1005–1026. https://doi.org/10.1029/2017GB005862

Weller, R., Schmidt, K., Teinilä, K., & Hillamo, R. (2015). Natural new particle formation at the coastal Antarctic site Neumayer. *Atmospheric Chemistry and Physics*, *15*, 11399–11410. https://doi.org/10.5194/acp-15-11399-2015

Woodhouse, M. T., Carslaw, K. S., Mann, G. W., Vallina, S. M., Vogt, M., Halloran, P. R., & Boucher, O. (2010). Low sensitivity of cloud condensation nuclei to changes in the sea-air flux of dimethyl-sulphide. *Atmospheric Chemistry and Physics*, *10*, 7545–7559. https://doi.org/10.5194/acp-10-7545-2010

Woodhouse, M. T., Mann, G. W., Carslaw, K. S., & Boucher, O. (2013). Sensitivity of cloud condensation nuclei to regional changes in dimethyl-sulphide emissions. *Atmospheric Chemistry and Physics*, *13*, 2723–2733. https://doi.org/10.5194/acp-13-2723-2013

Yoon, Y. J., & Brimblecombe, P. (2002). Modeling the contribution of sea salt and dimethyl sulfide derived aerosol to marine CCN. *Atmospheric Chemistry and Physics*, *2*(1), 17–30. https://doi.org/10.5194/acp-2-17-2002

Zhang, M., Park, K.-T., Lin, Q., Yan, J., Park, K., Wu, Y., et al. (2020). Atmospheric dimethyl sulfide and its significant influence on the sea-to-air flux calculation over the Southern Ocean. *Progress in Oceanography*, *186*, 102392. https://doi.org/10.1016/j.pocean.2020.102392

Zheng, G., Wang, Y., Wood, R., Jensen, M. P., Kuang, C., McCoy, I. L., et al. (2021). New particle formation in the remote marine boundary layer. *Nature Communications*, *12*(1), 527. https://doi.org/10.1038/s41467-020-20773-1